Spatial variation of subduction zone fluids during progressive subduction : Insights from Serpentinite Mud Volcanoes

Catriona D. Menzies, Roy E. Price, Jeffrey Ryan, Olivier Sissmann, Ken Takai, C. Geoffrey Wheat

HAL Id: hal-03910016
https://ifp.hal.science/hal-03910016

Submitted on 21 Dec 2022

Spatial variation of subduction zone fluids during progressive subduction: Insights from Serpentinite Mud Volcanoes

Catriona D. Menzies [a,*], Roy E. Price [b], Jeffrey Ryan [c], Olivier Sissmann [d], Ken Takai [e], C. Geoffrey Wheat [f]

[a] *Department of Earth Sciences, Durham University, Science Laboratories, South Road, Durham DH1 3LE, UK*
[b] *SUNY Stony Brook, School of Marine and Atmospheric Sciences, Stony Brook, NY, USA*
[c] *Department of Geology, University of South Florida, Tampa, USA*
[d] *IFP énergies nouvelles, 92500 Rueil-Malmaison, France*
[e] *Institute for Extra-cutting-edge Science and Technology Avant-garde Research (X-star), Japan Agency for Marine-Earth Science Technology (JAMSTEC), Yokosuka, Japan*
[f] *College of Fisheries and Ocean Sciences, University of Alaska Fairbanks, PO Box 475, Moss Landing, CA 95039, USA*

Abstract

Geological processes at subduction zones control seismicity, plutonism and volcanism, and geochemical cycling between the oceans, crust, and mantle. The down-going plate experiences metamorphism, and the associated dehydration and fluid flow alters the physical properties of the plate interface and mantle wedge, as well as controlling the composition of material descending into the mantle. Any direct study of slab evolution during subduction is inhibited by the prohibitive depths at which these processes occur. To examine these processes we use serpentinite mud volcanoes in the Mariana forearc, that permit sampling of serpentinite materials and their pore waters that ascend from the subduction channel. We present new pore water chemical data from the summit and flanks of three serpentinite mud volcanoes that were drilled during International Ocean Discovery Program Expedition 366 which are reflective of reactions within the crust and mantle during the early, shallow (<20 km) stages of subduction. We show, via thermodynamic modelling, that our new data on the evolution of pore water chemical compositions reflect mineralogical characteristics of a predominately basaltic source from the downgoing Pacific Plate. However, a component from sedimentary sources is likely, especially for those mud volcanoes near the trench. Other potential slab-derived constituents, such as lithospheric serpentinite, carbonate-rich sediments, or seamount basalts with an intraplate geochemical character, are not required to explain our results. Our results indicate that with progressive subduction the lawsonite-epidote mineral transformation boundary at ~250 °C may help drive slab carbonate destabilisation, despite its apparent thermodynamic stability at such temperatures and projected pressures (~300 °C and ~0.6 GPa). New dissolved gas data also point to primary thermodynamic controls over methane/ethane production within the subduction channel as depths-to-slab increase. Our findings provide direct evidence for the progressive mineralogical and chemical evolution of a subducting oceanic plate, which liberates a progressively evolving fluid phase into the subduction channel.
© 2021 The Authors. Published by Elsevier Ltd. This is an open access article under the CC BY license (http://creativecommons.org/licenses/by/4.0/).

Keywords: Serpentinite; Mud volcanoes; Mariana forearc; Subduction; Geochemical cycling; Devolatilization

* Corresponding author.
  E-mail address: catriona.d.menzies@durham.ac.uk (C.D. Menzies).

1. INTRODUCTION

Subduction of oceanic crust is one of the primary processes that shape the seafloor, return elements to the mantle (Bebout, 2007), and trigger some of the largest earthquakes on Earth (Moore and Saffer, 2001; Henstock et al., 2006). What we know of subduction processes stem largely from geophysical data and scientific ocean drilling, which has been used to quantify inputs and constrain outputs in arc settings (Alt and Teagle, 1999; Kerrick and Connolly, 2001a, b; Savov et al., 2005; Plank and Manning, 2019). However, between the trench and arc there is generally a void of physical samples to assess the state of water-rock-sediment reactions, thermal and pressure conditions, and physical properties of materials within the subduction channel. Our understanding of this transition zone at a nonaccretionary convergent margin is possible through studies of the Mariana forearc (Fryer, 1996). Here across- and along-strike extension and vertical tectonic deformation produce faults, some of which penetrate the overriding Philippine Plate into the subduction channel below (Fryer and Salisbury, 2006; Fryer et al., 2020). Conduits form where such faults intersect, forming a pathway for fluids, clasts of rock from the subduction channel and mantle wedge, and a serpentinite matrix to be transported from the subduction channel to the seafloor. This transport of material results in large (up to 50 km wide and 2 km high) serpentinite mud volcanoes (Fryer, 2012). Thus, these serpentinite mud volcanoes provide a window into the chemical, thermal and physical conditions within the subduction channel during the initial to intermediate stages (10–20 km depth) of subduction (Fryer et al., 1999).

Numerous serpentinite mud volcanoes are documented in the Mariana forearc, sited at different distances from the trench, and by supposition reflecting different temperature and pressure conditions beneath them within the subduction channel (Fryer and Fryer, 1987, Fryer, 2012; Ichiyama et al 2021) (Fig. 1). Thus, by sampling different serpentinite mud volcanoes one can determine the evolution of fluids and materials in the subduction channel as they descend and warm with distance from the trench (Wheat et al., 2020). By understanding the evolution of these materials we can, for example, better understand processes of devolatilization of the down-going plate, which is fundamental to models for subduction-related metamorphism and backarc magmatism (Tatsumi and Eggins, 1995; Bebout, 2007; Ryan and Chauvel, 2014). As devolatilization occurs at depths greater than the current ability to drill, much of our understanding of slab devolatilization phenomena is largely founded on inferences from elemental and isotopic systematics in arc volcanic rocks and exhumed metamorphic massifs, experimental studies of fluid-rock-melt exchanges, and thermodynamic calculations (e.g., Kessel et al., 2005; Bebout et al., 2007; Marschall et al., 2007; Schmidt and Poli, 2014). The serpentinite mud volcanoes allow us to study such processes during the early to intermediate stage of subduction.

To better understand early to intermediate subduction-related processes, International Ocean Discovery Program (IODP) Expedition 366 cored three active serpentinite
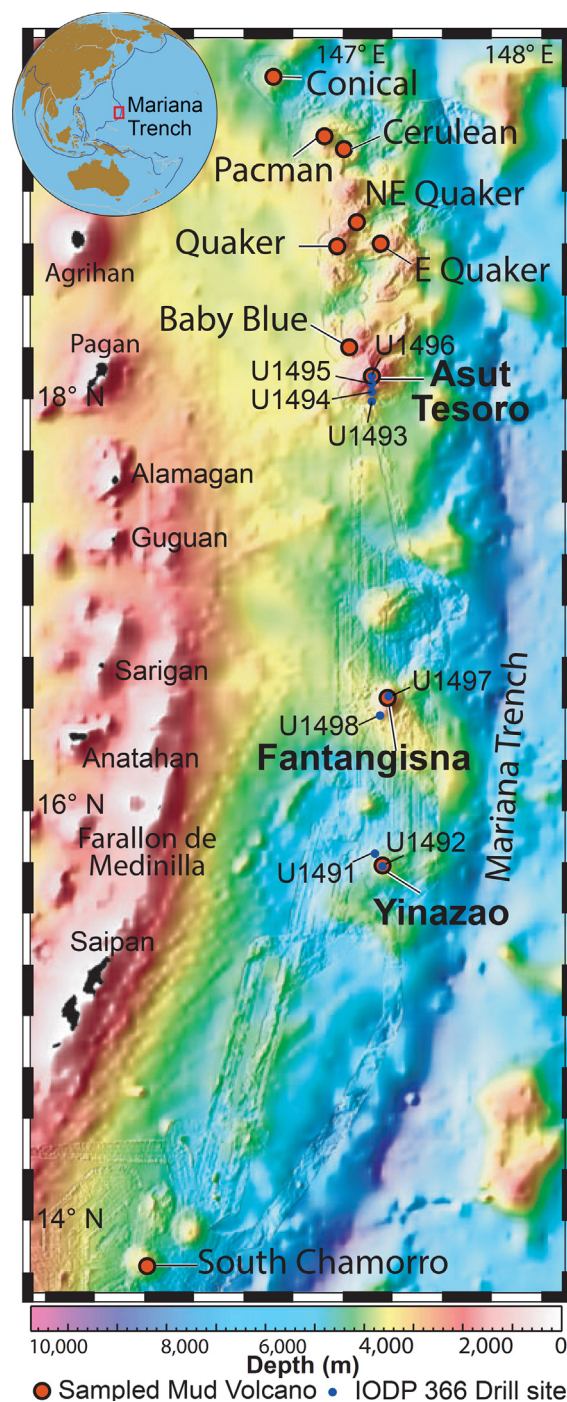
Fig. 1. A bathymetric map of the Mariana forearc and insert placing the Mariana forearc within the broader context of the Pacific Ocean. Mud Volcano locations of those newly drilled on IODP Expedition 366 (in bold, with drill sites labelled) and those previously sampled as summarised in Table 1 are labelled.

mud volcanoes in the Mariana forearc (Fig. 1). The primary goals for the expedition were to (1) constrain mass transport processes, (2) elucidate the spatial variability of slab-related fluid in the context of reaction within the subduction channel, (3) characterize the metamorphic and

tectonic history within and along the subduction channel, and (4) constrain metabolic potential and activity of extant microbial communities. Here we report pore water solute and dissolved gas data from the summits of three serpentinite mud volcanoes to address several of these goals with an emphasis on the chemical evolution of slab fluids within the subduction channel. Each of the three serpentinite mud volcanoes is active, but they are active to different degrees. Thus, all three provide a measure of the composition of the deep-sourced fluids that feed the serpentinite mud volcanoes at different distances (and by proxy depth and temperature) from the initiation of plate subduction. We also sampled several sites on the flanks of these three serpentinite mud volcanoes where older serpentinite flows are covered by more recent ones. Pore water data from these areas provide a measure of continued serpentinization, diffusive exchange with bottom seawater, and potential for reactions that affect material properties and microbial metabolic activity. We also sampled a third environment, which is the pelagic sediment that resides under these serpentinite mud volcanoes. As mass wasting of serpentinite flows spread with continued inputs through a central conduit the surrounding pelagic sediment is covered with serpentinite. These underlying pelagic sediments are affected by diffusive exchange with the overlying serpentinite flows, affecting potential metabolic rates and pathways of resident microbial communities.

2. SITE DESCRIPTION

Three serpentinite mud volcanoes were cored on IODP Expedition 366; Yinazao Seamount (formerly called Blue Moon Seamount), Fantangisna Seamount (formerly Celestial Seamount) and Asùt Tesoru Seamount (formerly Big Blue Seamount) (Fig. 1). Combined with results from South Chamorro and Conical Seamounts (Ocean Drilling Program (ODP) Exp. 125, Fryer et al., 1990; ODP Exp. 195, Salisbury et al., 2002) these five serpentinite seamounts form a transect with (1) distance from the trench, (2) depth and temperature to the subduction channel, and (3) composition of deep-sourced fluids. The three serpentinite mud volcanoes drilled during IODP Exp. 366 also differ in their level of mudflow activity, which could affect conditions on the flanks of the seamount. Much more detail of these three volcanoes is provided in Fryer et al. (2018), but for completeness we outline geologic characteristics for each of the serpentinite mud volcanoes that were cored during IODP Exp. 366.

Yinazao Seamount is ∼1 km high and ∼55 km from the trench with a depth to slab of 13 km and temperature on the slab estimated at ∼80 °C, at sub-greenschist facies/prehnite-pumpellyite metamorphic conditions (Hulme et al., 2010; Oakley et al., 2007; Oakley et al., 2008; Ichiyama et al., 2021) (Fig. 1). Fluid discharge in excess of the serpentinite material was discovered in an area of deformation along the southwest edge of the summit region (IODP Site U1492) (Hulme et al., 2010). Deep-sourced fluids that discharge from this site have higher calcium concentrations and lower alkalinity than bottom seawater. However, because fluid seepage was sufficiently slow, the

deep-sourced fluid composition was not defined in earlier studies (Hulme et al., 2010). One flank site (IODP Hole U1491) was cored on the northwest side to characterize one of the oldest flows that had not been affected by a "recent" mass-wasting event.

Fantangisna Seamount is ∼1.5 km high and 62 km from the trench with a depth to slab of 14 km and estimated temperature in the slab of ∼150 °C at greenschist facies metamorphic conditions (Hulme et al., 2010; Oakley et al., 2008) (Fig. 1). The summit depression is consistent with slope failure to the north-northwest. Fluid seepage was discovered along the headwall of the scarp where deep-sourced fluids were recovered at a depth of 40 cm (IODP Site U1497) (Hulme et al., 2010). However, fluid seepage was sufficiently slow such that the composition of the deep-sourced fluid was not constrained. IODP Site U1498 was located on the southeastern flank where serpentinite flows thin to several hundred meters above pelagic sediment, which was recovered in two holes.

Asùt Tesoru Seamount is 72 km from the trench with a depth to slab of 18 km and estimated temperature in the slab of ∼250 °C, at blueschist facies metamorphic conditions (Hulme et al., 2010; Oakley et al., 2008; Ichiyama et al 2021) (Fig. 1). This is one of the largest serpentinite mud volcanoes in the forearc, spanning 50 km in width and 2 km in height (Fryer, 1996). The summit region has a distinct circular knoll in which the fluid discharge rate was the highest in the middle of the feature and decreased with distance from the center (IODP Site U1496) (Hulme et al., 2010). These deep-sourced fluids have lower calcium and higher alkalinity concentrations than bottom seawater. Three flank sites were cored to the south of the summit knoll with IODP Site U1495 at the rim of the summit, Site IODP U1494 about midway down the seamount, and IODP Site U1493 near the base of the seamount.

3. SAMPLE COLLECTION AND ANALYTICAL METHODS

Sample collection and analysis followed standard IODP protocols and are described in detail elsewhere (Fryer et al., 2018; Wheat et al., 2018). For completeness, we outline sample collection and analyses protocols here. Serpentinite muds were recovered primarily using the half-length advanced piston corer (HLAPC), but some cores were recovered using the extended core barrel (XCB) and rotary core barrel (RCB) coring systems. Serpentinite material and sediment for pore water extraction were immediately taken from whole-round sections that were 10 to 40 cm in length. These whole rounds were cooled to 2–5 °C, which was the *in situ* temperature, before processing. Serpentinite and sediment samples were then extracted from the core liner in a nitrogen-filled glove bag, scraped to remove the outer contaminated rind, and placed in a titanium squeezer above a pre-washed Whatman No. 1 filter. The squeezer was removed from the glove bag and inserted into a laboratory hydraulic press. Pore waters were expelled at pressures <30 MPa, filtered (0.45 μm), aliquotted, preserved, and stored. A total of 149 pore water samples were collected and analyzed.

Pore water analytical techniques were based on those outlined by Gieskes et al. (1991) and Murray et al. (2000), and updated in Wheat et al. (2018) and Fryer et al. (2018). Pore waters were analyzed for: (1) pH (25 °C) and alkalinity using a pH electrode and titrating with HCl; (2) chloride, sulfate, bromide, and Na using an ion chromatographic (IC) technique; (3) chlorinity by titrating with a AgNO$_3$ solution using a silver selective electrode after diluting a 100 μl sample in nitric acid to mobilize volatile hydrogen sulfide; (4) ammonium, phosphate, and dissolved sulfide using spectrophotometry techniques; (5) the major and minor cations using two different dilutions prior to injection into an inductively coupled plasma-optical emission spectrometer (ICP-OES); (6) and dissolved inorganic and organic carbon (DIC and DOC) analysis using an OI Analytical Aurora 1030C total organic carbon (TOC) analyzer. Because of the high Ca and Sr concentrations additional standards with 6 times the seawater Ca and 8 times the seawater Sr were used. Because of the lack of sensitivity in the Li and Ba measurements at sea, we analyzed most of the samples ashore using ICP-OES methods consistent with results that were generated from these and other sampling of serpentinite mud volcanoes (e.g., Hulme et al. 2010; Mottl et al. 2004). Results from these shore-based analyses and shipboard results agree within analytical precision (Wheat et al., 2018). Additional trace elements (Ba, Rb, Cs, V, Mo, and U) were analyzed by inductively coupled plasma-mass spectrometer (ICP-MS) (Wheat et al., 2018).

To quantify concentrations of H$_2$, CO, CH$_4$, C$_2$H$_6$, and C$_3$H$_8$, 1 cm^3 of unconsolidated material was collected from the freshly exposed end of the core after the core was brought on deck and sectioned. This sample was placed in a 20-cm^3-glass vial with 3 mL of distilled water and a small amount of HgCl$_2$ to prevent microbial activity. The vial was sealed with a Teflon-coated butyl rubber septum and a crimped aluminum cap then placed in the oven at 80 °C for 30 minutes. A 0.5 cm^3 aliquot of the evolved gases was extracted from the headspace vial with a standard gas syringe and automatically injected into a GL Science GC4000 gas chromatograph (GC) equipped with a helium ionization detector (HID) set at 250 °C. The column (2 mm inner diameter; 6.3 mm outer diameter) was packed with carbosieve (Agilent/Hewlett Packard). The GC oven was set to remain at 40 °C for 5 min with a subsequent rise to 250 °C at a rate of 20 °C min^{-1}. In addition, another 0.5 cm^3 aliquot of the evolved gases was automatically injected into an Agilent/Hewlett Packard 6890 Series II GC equipped with a flame ionization detector (FID) set at 250 °C. The column (2 mm inner diameter; 6.3 mm outer diameter) was packed with 80/100 mesh HayeSep (Restek). The GC oven was set to remain at 80 °C for 8.25 min with a subsequent rise to 150 °C at a rate of 40 °C min^{-1}. The chromatographic response was calibrated using two gas standards. Concentrations of dissolved H$_2$S were determined from 1 cm^3 of sediment from the exposed end of the core directly after the core was cut. This aliquot of sediment was placed in a 20-cm^3-glass vial and slurried in 3 ml of 1 N HCl solution with a Teflon-coated butyl rubber septum. The slurried sample was measured using an electrochemical H$_2$S probe (H$_2$S-40 N, Unisense, Denmark). The H$_2$S concentration was calibrated using seawater containing 10 mM Na$_2$S solution acidified by 1 N HCl seawater at the same temperature.

4. RESULTS

4.1. Summit sites (U1492, U1496, U1497)

We outline three striking characteristics of the pore water data from summit sites. The first characteristic is the range in concentrations and the systematic differences in fluid compositions. For example, pH (25 °C) values in pore waters from Fantangisna (U1497) and Yinazao (U1492) increase with depth to a value of less than 11, whereas pore waters from Asùt Tesoru (U1496) reach a pH (25 °C) of 12.5 (e.g., Fig. 2). Similarly, the two seamounts that are closer to the trench (Yinazao and Fantangisna) have lower alkalinities and higher dissolved Ca and lower Na (Fig. 3) concentrations than pore waters more distal from the trench (Asùt Tesoru). Data from Asùt Tesoru provide a closer match to data from previous drilling expeditions on South Chamorro and Conical Seamounts (Mottl, 1992; Mottl et al., 2003; Wheat et al., 2020), both to the west of the transect of seamounts drilled during IODP Exp. 366 and further from the trench (at depths to slab of 18 and 19 km respectively).

A second striking characteristic is illustrated with the alkali metals data (Fig. 3). These data highlight differences among the sites and calculated deep-sourced fluids from South Chamorro and Conical Seamounts (Mottl, 1992; Mottl et al., 2003; Wheat et al., 2020). Except for Li, the remaining alkali metals that were measured have a distinctly different concentration in pore waters from Asùt Tesoru than Yinazao and Fantangisna and are more closely related, but distinctly different from South Chamorro and Conical Seamounts.

Lastly, the head-space gas concentrations of dissolved hydrogen and methane at Yinazao and Fantangisna are distinctly different from those at Asùt Tesoru (Fig. 4; Fig. 3 of Eickenbusch et al., 2019). Degassing of cores from Asùt Tesoru resulted in voids within the cores and a high background methane concentration in the laboratory where the cores were split and opened for display and sampling.

The summit regions of most of the Mariana serpentinite mud volcanoes have pore water seepage rates that exceed the serpentinite matrix (Fryer et al., 1999; Hulme et al., 2010; Mottl et al., 2003; Mottl et al., 2004). This conclusion was based on comparing pore water chemical profiles to simulations of a simplified transport (advection and diffusion) equation utilizing a range of advective rates. Whereas these models could be used to constrain seepage rates utilizing data from IODP Exp. 366, prior surveys with better spatial (depth and distance) resolution within the first meter of sediment provide a better measure of the seepage rate at summit sites. This seepage rate was typically several to tens of centimeters per year for most of the summit sites (Hulme et al., 2010). The significant aspect of such models in relationship to the IODP Exp. 366 data is that such models define the deep-sourced endmember as the asymptotic
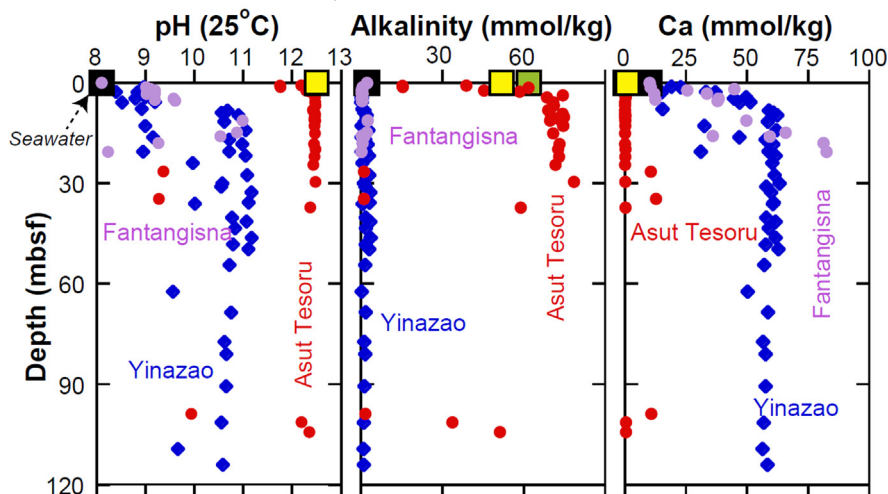
Fig. 2. pH (25 °C), alkalinity and Ca in pore waters extracted from cores that were collected from the summit of Yinazao (U1492), Fantangisna (U1497), and Asùt Tesoru (U1496) Seamounts, each a serpentinite mud volcano. Black squares, light green squares and yellow squares denote concentration in bottom seawater, deep-sourced fluid from South Chamorro Seamount (Wheat et al., 2020), and deep-sourced fluids from Conical Seamount (Mottl, 1992), respectively. Note, samples with lower pH represent mixing with seawater in the upper parts of the sediment and/ or during core retrieval.
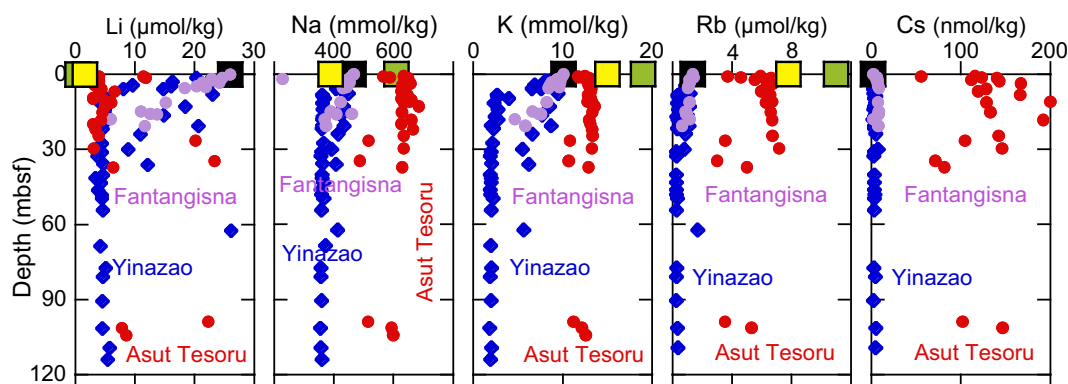

Fig. 3. Alkali metal (Li, Na, K, Rb, Cs) concentrations in pore waters from cores collected from the summit of Yinazao (U1492), Fantangisna (U1497), and Asùt Tesoru (U1496) Seamounts, each a serpentinite mud volcano. Black squares, light green squares and yellow squares denote concentration in bottom seawater, deep-sourced fluid from South Chamorro Seamount (Wheat et al., 2020), and deep-sourced fluids from Conical Seamount (Mottl, 1992), respectively.

concentration as a function of depth. Thus, a measure of the deep-sourced fluid composition can be determined from concentration-depth profiles from two of the three seamounts that were cored during IODP Exp. 366. However, on the third, Fantangisna, seamount, we were unable to core deep enough to reach the asymptotic composition, thus we provide an estimate for the deep-sourced fluid at this site (Table 1). We compiled the composition of deep-sourced fluids from the three seamounts that were cored during IODP Exp. 366 and other Mariana serpentinite mud volcanoes to assess trends that could be used to interpret conditions in the subduction channel as the Pacific Plate descends (Table 1). This is an internally consistent data set derived from pore water data; however, because of artifacts induced during sampling and handling sediment to recover pore waters, some of these values may be slightly

different than fluids obtained with artifact-free techniques (e.g., Wheat et al., 2008 and 2020).

4.2. Flank sites (U1491, U1493-95 and U1498) and pelagic sediment (U1498)

If the chemical compositions of pore water from flank sites was a relic of the deep-sourced fluid during emplacement, potential mixture with bottom seawater during mass wasting, and diffusion with bottom seawater after deposition, then plots of conservative ions should show a linear response with data spanning the two endmembers (bottom seawater and deep-sourced fluid). Pore water compositions from summit sites mostly follow this general condition, defined by mixing (diffusively) between the deep-sourced fluid and bottom seawater (Fig. 5). However, chemical data
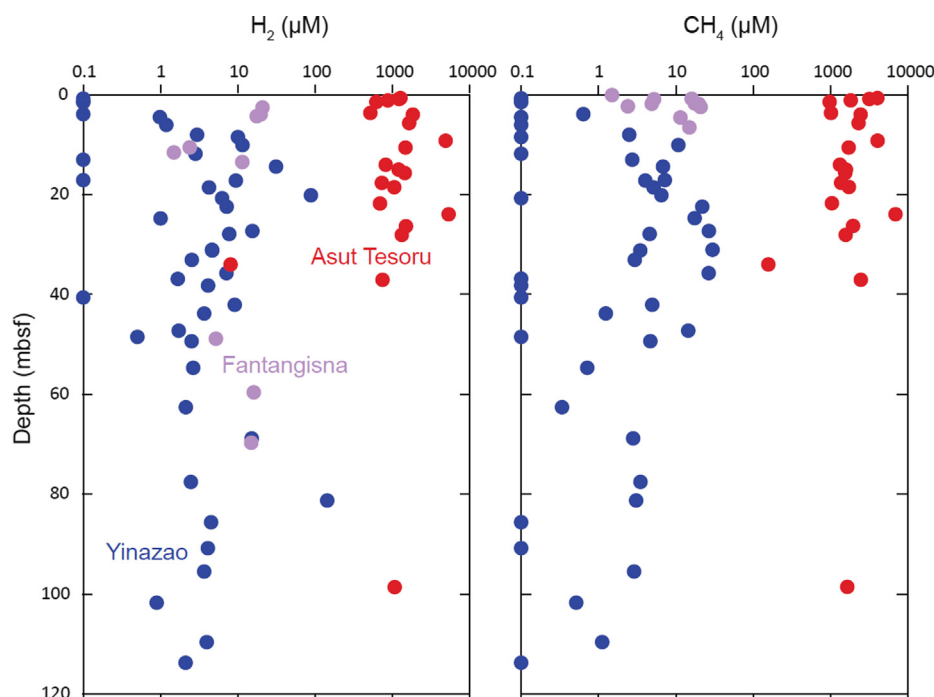
Fig. 4. Dissolved hydrogen and methane concentrations in head space gases, cores collected from the summit of Yinazao (U1492), Fantangisna (U1497), and Asùt Tesoru (U1496) Seamounts, each a serpentinite mud volcano. Bottom seawater (not shown) has concentrations that are below detection for dissolved hydrogen and methane. *Data from* Eickenbusch et al., (2019).

from flank sites do not necessarily follow these linear trends, indicating reactions that are post-depositional. In the case of the summit sites, reaction is limited to the serpentinite matrix. In contrast, on the flanks mass-wasting events can incorporate or cover pelagic sediment that was deposited between mass wasting events. Thus, it is not surprising that pore water chemical data from flank sites show more complex relationships with depth than samples from summit sites.

More reactive solutes and pH (25 °C) data are shown in Fig. 6 with an indication of the deep-sourced fluid at each of the three summits. For example, Ca concentrations on the flanks of Asùt Tesoru (IODP Sites U1493 and U1494) are significantly greater than the deep-sourced fluid, indicating a source of Ca, which, in part, stems from reaction between the matrix and bottom seawater. Because of the elevated Ca values, the alkalinity is less than 1 mmol kg^{-1} and the pH (25 °C) is about 9, relative to the deep-sourced fluid from this site with a pH (25 °C) of 12.5.

Reactions that occur on the flanks can be more complex, especially near the distal end of the seamount. For example, IODP Hole U1498A penetrated 53 m of serpentinite matrix and 128.6 m of pelagic-volcanic sediment and IODP Hole U1498B, closer to the summit, penetrated 205 m of serpentinite matrix and 55 m of pelagic-volcanic sediment below. These two holes reflect markedly different conditions in terms of their interstitial water chemical profiles (Fig. 6). Pore water chemical concentrations from IODP Hole U1498A are more similar to bottom seawater, whereas data from IODP Hole U1498B have pH (25 °C) values that are consistently above 10.8 at depths greater than 50 meters

below seafloor (mbsf). At IODP Hole U1498A pore waters have a seawater-dominated signature upon which diagenetic reactions with serpentinite muds, xenoliths/ clasts, sands, and modified sediments impart changes to some solute profiles. In contrast, IODP Hole U1498B and ODP Hole 779A, which was positioned on the flank of Conical Seamount (ODP Leg 125, Mottl, 1992), have interstitial water pH (25 °C) values that are consistently > 10.5 at depths greater than 50 mbsf. Torishima Seamount, an inactive serpentinite seamount, had pH (25 °C) values of only 9.6 (Mottl, 1992).

5. DISCUSSION

5.1. Conditions at the slab-mantle interface beneath the Mariana serpentinite mud volcanoes

Initial investigations of the chemical composition of deep-sourced fluids in serpentinite mud volcanoes constrain temperatures within the subduction channel and were correlated to the distance from the trench (Fryer et al., 1999; Mottl et al., 2004; Hulme et al., 2010) (Fig. 7A). If the dip and thickness of subducting Pacific Plate was uniform, then distance from the trench would provide a good proxy for depth within the subduction channel. However, the incoming Pacific Plate supports many seamounts and guyots (Fryer et al., 2020). As these kilometer-tall features subduct, they affect the overlying Philippine Plate, causing topographic highs and seafloor deformation (Fryer et al., 2020). This deformation likely alters the depth (temperature) of the subduction channel (Stern and Smoot, 1998). An indication of this disruption is the presence of limestone

Table 1
Summary of the chemistry of deep-sourced fluids. nd = not determined. * = Expedition 366 data are the average of deeper samples at the summit sites, as described in the text, full analystical data can be accessed at: https://doi.org/10.14379/iodp.proc.366.2018. Other data are from Hulme et al., 2010.

Seamount	Bottom seawater	Yinazao (Blue Moon)*	Cerulean Springs	East Quaker	Fantangisña (Celestial)*	NE Quaker	Pacman	Quaker	Baby Blue	Asùt Tesoro (Big Blue)*	South Chamorro	Conical
Distance to trench (km)	0	55	60	61	62	63	70	76	72	72	78	86
pH	8.1	10.7	10.8	10.7	~10.8	>8.3	>8.9	9.2	>9.0	12.5	12.5	12.5
Alkalinity (mmol/kg)	2.3	1.4	2.3	3.1	<0.5	<1.3	<1.0	0.8	<1.0	73	62	52
Mg (mmol/kg)	52.4	0.9	0	0.2	<2	20	44	0.5	40	0.8	0	0.1
Ca (mmol/kg)	10.2	58	49.5	74.8	>82	>33	<6.9	18.1	<6.9	0.1	0.3	1
Sr (µmol/kg)	90	750	320	nd	>630	nd	<56	205	<61	13	10	20
Sulfate (mmol/kg)	28	23.9	8.5	6.9	<8	<23	<25	23	<22	30	28	46
Ba (µmol/kg)	0.14	0.22	0.297	nd	~0.8	nd	<0.118	0.125	0.22	0.07	0.4	0.1
B (µmol/kg)	410	0.2	15	nd	<1	nd	<387	830	nd	1070	3000	3900
Li (µmol/kg)	26	4.7	2.1	nd	~12	nd	>30.3	119	>31	4	0.4	1.6
Na (mmol/kg)	466	361	220	360	~400	<420	464	461	>489	640	610	390
K (mmol/kg)	10.1	0.9	2.2	3.7	<6	<7.64	10.1	9.39	10.5	13	19	15
Rb (µmol/kg)	1.37	0.29	0.45	nd	<1	nd	>1.4	1.57	>1.69	6.6	10	7.8
Cs (nmol/kg)	2.2	3.6	5.6	nd	~7.7	nd	>9.1	96	>10.3	160	53.5	>61.6
V (nmol/kg)	38.4	16	25.1	0.8	~15	40.7	nd	80.3	5.4	100	16.3	113
Mo (nmol/kg)	100	10	20	198	~4	50	nd	36	198	104	24	42
U (nmol/kg)	13.5	0.08	0.31	nd	0.1	nd	<0.28	0.01	<0.54	0.3	<0.1	0
Phosphate (µmol/kg)	–	2	nd	nd	<0.5	nd	nd	nd	nd	3	nd	nd
Ammonium (µmol/kg)	–	95	nd	nd	~3	nd	nd	nd	nd	180	nd	nd

from a Cretaceous seamount that was subducted, then transported to the seafloor where it was cored on Yinazao (Fryer et al., 2020). Instead, studies of the mineralogy of erupted clasts from the subducting slab and forearc mantle are used to constrain pressure–temperature conditions beneath the mud volcanoes in the Mariana forearc.

The mineralogy of erupted clasts across the Mariana forearc describes spatial mineralogical changes associated with increasing depth to subducting slab westwards (Ichiyama et al., 2021). The two main clast types recovered are metabasites and serpentinite/ ultramafic rock and the mineralogy of these have been documented across the Mariana forearc. The serpentinite clast mineralogy changes from dominantly lizardite/ chrysotile at Yinazao (13 km depth) to lizardite/ chrysotile to antigorite at Fantangisna (14 km depth) to antigorite at Asùt Tesoru and Conical (18 and 19 km depth), outlining increasing metamorphic grade with depth (Murata et al., 2009; Ichiyama et al., 2021). The metabasite clasts reveal a similar pattern of increasing metamorphic grade with depth to slab; from zeolite to prehnite-pumpellyite at Yinazao, to prehnite-pumellyite at Fantangisna to lawsonite-blueschist containing jadeitic pyroxene and aragonite at Asùt Tesoru (Ichiyama et al., 2021), lawsonite-blueschist at Conical (Maekawa et al., 1993), to epidote-blueschist at South Chamorro (Tamblyn et al., 2019). Amphibolite clasts that document higher temperature metamorphism than the present day, associated with Eocene subduction initiation (Ichiyama et al., 2021), are overprinted with the same mineral assemblages documented in the metabasic clasts, and have likely resided in the subduction channel since initia-

tion (Tamblyn et al 2019, Ichiyama et al., 2021). However, the progressive and systematic change in HP/LT metamorphic grade with depth to slab, which agrees with geophysical survey estimates of depth/ pressure (Ichiyama et al., 2021) of 0.3, 0.4 and 0.6 GPa for Yinazao, Fantangisna and Asùt Tesoru respectively (Oakley et al., 2008) indicates that the modern day plumbing of the forearc mud volcanoes directly samples the slab-mantle interface beneath each mud volcano and records the present day thermal structure of the subducting slab (Ichiyama et al., 2021).

5.2. Trends in deep-sourced solute composition and source

We cannot directly measure thermal conditions within the subduction channel; however, we can use solute and mineralogical data as proxies for temperature. Here we use potassium concentrations as a proxy for increased temperature with subduction. Potassium data are ideally suited, because the only source of K in ascending pore waters is the down-going plate and K mobility is temperature sensitive to water-basalt reactions (Mottl et al., 2004). For example, laboratory experiments show K concentrations are consumed by secondary minerals at temperatures < 150 °C and K is released from the basaltic matrix at temperatures > 150 °C (Seyfried and Bischoff, 1979). Similarly, Rb and Cs concentrations in deep-sourced fluids also are temperature sensitive in water–rock and water–sediment experiments (James et al., 2003; You et al., 1996). When the Rb fluid data estimated from the subduction channel are plotted versus K, a monotonic trend emerges (Fig. 7B). In contrast, the Rb data plotted versus distance
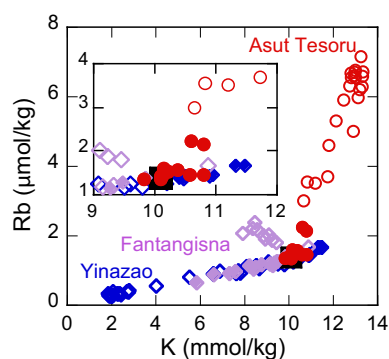
Fig. 5. Potassium versus rubidium in pore waters from IODP Exp. 366 with the inset focused around the seawater value (black filled square). Open symbols represent samples from summit sites (U1492, U1496, U1497). Filled symbols represent samples from flank sites (U1491, U1493-5, U1498). Simple mixing of an endmember deep-sourced fluid (Asùt Tesoru top right; Yianzao and Fantangisna bottom left and middle shown by open symbols) with seawater (black square) would define a linear response. Most of the data are consistent with simple mixing with some exceptions, especially material from the flanks of Fantangisna where we collected pelagic sediment below serpentinite flows. These data illustrate that for even some relatively non-reactive solutes, water–rock reactions occur in the serpentinite matrix on the flanks of the seamount.

(not shown) from the trench are not monotonic. Thus, the chemical data may account for irregularities in thermal conditions at depth that are caused by heterogeneous inputs at the trench. The Cs data plotted versus K does not result in a monotonic trend, suggesting that reactions within the crust are a complex mixture of water–rock and water sediment reactions, the latter has a greater impact on the fluid's Cs concentration than Rb with rising temperatures (James et al., 2003; You et al., 1996).

Other solutes, such as B concentrations, also show a temperature dependence on the deep-sourced fluid composition resulting from water-rock and water–sediment experiments (Seyfried and Bischoff, 1979; You et al., 1996; James et al., 2003). In the subduction channel of the Mariana fore-

arc, B concentrations are < 5% of the seawater value in low K fluids and an order of magnitude higher than seawater when K concentrations are greater than seawater (Fig. 7C). Water-rock and water–sediment experiments have shown a stronger liberation of B from sediment than from basalt (James et al., 2003), endorsing our earlier suggestion that the fluid is a mixture of sediment and basaltic influences.

In contrast, Ca concentrations decrease with increasing K concentrations with the highest three K concentrations having depleted Ca values and high alkalinities. It is to be noted that erupted mafic clasts within serpentinite muds at all mud volcano sites show evidence for rodingisation (Fryer et al., 2018) suggesting this is a ubiquitous phenomenon. Such rodingisation may affect the concentrations of pore water Ca, Sr, K and Rb. However, we note there are significant changes in K, Rb and Ca across the different mud volcanoes, and as these processes are evident everywhere, we conclude that the rodingite effect is secondary and does not control the systematic trends we note. Instead, the removal of Ca is consistent with active decarbonization of the subducted plate as the plate descends and warms (Fig. 7C; Fryer et al., 1999; Wheat et al., 2020). This works in tandem with the exchange of Ca for Na with increasing temperature and pressure (Seyfried et al., 2007; Wheat et al., 2020), resulting in a higher solute Na concentration at warmer temperatures, even accounting for dilution (e.g., Na/Cl in Fig. 7D, 8). Unlike the other alkali metals, the Li data are generally much lower than seawater, with the exception of when the K data are about at seawater values (Fig. 7D), suggesting that Li may undergo further reactions as the fluids ascend into the overriding plate.

Extensive serpentinization in the forearc mantle may affect the concentration of some elements in the erupted pore fluids. It follows that elements incompatible in the serpentine crystal structure, such as Ca, may be enriched in the fluid, and those that are compatible, e.g. B, are depleted. The minerals that are getting serpentinised are primarily olivine and enstatite; typically olivine contains ∼ 0.1 wt.% Ca, and while enstatite may have a few percent CaO, it makes up 10–15% at most of the hydrating peridotite
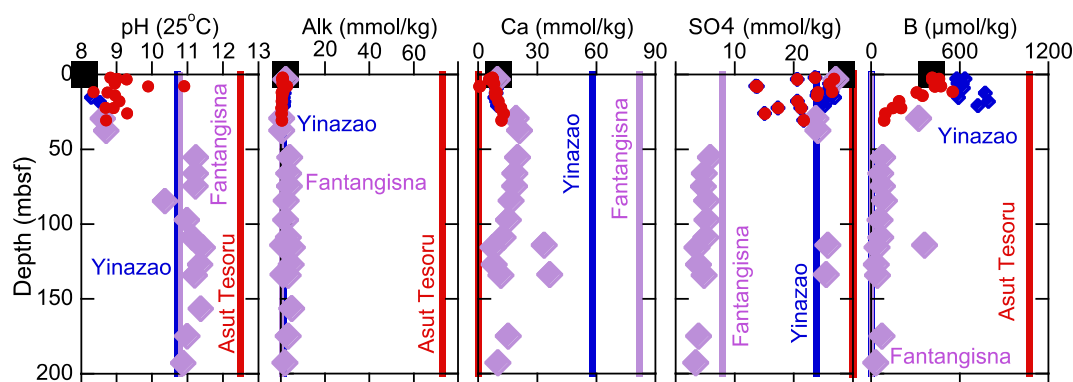

Fig. 6. pH (25 °C), alkalinity, Ca, sulfate and B concentrations in pore waters from cores collected from the flanks of Yinazao (U1491), Fantangisna (U1498), and Asùt Tesoru (U1493-5) Seamounts. Black squares denote concentration in bottom seawater. Vertical lines represent the composition of deep-sourced fluids. Some data trend towards the deep-sourced endmember whereas other do not, highlighting on-going reactions after deposition.
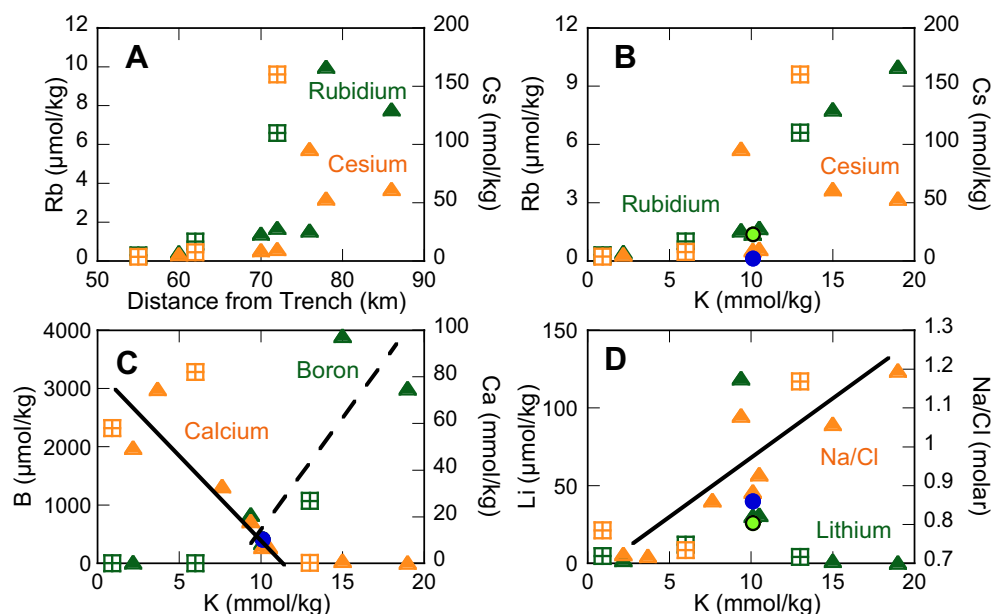
Fig. 7. Concentrations of deep-sourced solutes as a function of distance from the trench and dissolved K concentrations. Blue circles represent seawater values for the orange data and light green circles represent seawater values for the green data. The seawater value for the B-K relationship lies under the seawater symbol of the B-K relationship. Filled triangles are data from Hulme et al. (2010). Squares with lines represent data from IODP Exp. 366. A. Rb and Cs are plotted as a function of distance to highlight the non-monotonic changes after 70 km from the trench. B. Rb and Cs are plotted as a function of K to highlight the monotonic increase in Rb with increasing K and but such a monotonic increase is not observed with Cs. C. A regression line (solid) highlights changes in Ca with increasing K values to seawater concentrations. Another regression line (dashed) highlights the relationship between B and K, above values of 7 mmol K kg^{-1}. D. Na concentrations increase linearly with K (black line), whereas the Li data are lower than the seawater concentration with the exception of K concentrations in the range of 9 to 11 mmol kg^{-1}.

assemblage. Despite this, many ultramafic-hosted hydrothermal systems have elevated concentrations of Ca (e.g. Ca-OH type waters first recorded by Barnes and O'Neil (1969)) owing to Ca-Mg exchange reactions that follow a linear relationship (Klein and Le Roux, 2020). Our results show Ca to be elevated above seawater concentrations in the two shallowest depth to slab mud volcanoes, and to be markedly depleted in the deepest three mud volcanoes. Mg concentrations are significantly lower than seawater values at both the shallow and deeply sourced mud volcanoes (<2 mmol/kg; Table 1). Sr variability mimics that of Ca with depth to slab, showing marked elevation in the shallower two seamounts and strong depletion in the deeper three, suggesting that the variability in these species are likely controlled by reactions that affect them both, such as carbonate or plagioclase breakdown, with Ca-Mg exchanges playing a less prominent role. Given that serpentinisation is a pervasive process across the forearc, we conclude that serpentinisation reactions are not the primary driver of the Ca variability that we see, though they may contribute to the elevated Ca in porefluids from the shallower seamounts.

Serpentinized ultramafic clasts recovered from IODP Exp. 366 have elevated concentrations of fluid mobile elements (Li, B, Rb, Sr, Cs, Ba) (Albers et al., 2020). Serpentinisation may thus have an effect on the concentrations of these elements in the pore waters, but it cannot explain the variability seen between mud volcanoes, a variability which is also recorded in the serpentinized clasts and is related to

changing conditions on the subducting slab (Albers et al., 2020). Serpentinisation is not expected to affect the pore water concentrations of Na or K owing to their inherently low concentration in mantle minerals and incompatibility in the serpentine crystal structure. Here we use these element concentrations in pore waters to investigate the possible reactions and temperatures in the subduction channel below.

To assess the contribution of basalt versus sediment in the subducted material to the deep-sourced fluid, we applied thermodynamic calculations using PHREEQC software (Parkhurst and Appelo, 1999) coupled with the EQ3/6 LLNL mineralogical database. These models were constructed to investigate fluid compositions at equilibrium with various rock and sediment mineral assemblages across the temperature range of 25 °C to 300 °C. Rock and sediment modal compositions (Table S1) were estimated from core analysis of ODP Leg 185 of recovered non-altered sediments (ODP Site 1149) and volcanic rocks (ODP Site 801, about 20% altered) from the Izu-Bonin arc (Plank et al., 2000). A total of five mineral assemblages were considered, from 100% rock to 100% sediment, with a 20:80, 50:50 and 80:20 ratio (Table S2). Modeled fluid compositions were calculated at 12 discrete steps of 25 °C, from 25 °C to 300 °C. Owing to the limitations of the model, i.e., that solid solutions of minerals are not well represented and the complex evolution of the Pacific Plate in the subduction channel as it ascends, we limit our discussion to major ions such as K, Ca and Na, each of which has been shown to

vary systematically with distance from the trench in the Mariana forearc (e.g., Table 1, Fig. 7).

Calculated concentrations generally trend with measured data, i.e. pore water K and Na concentrations increase and Ca concentrations decrease with increasing temperature (Fig. 8). However, trajectories vary for different rock and sediment mixtures. The assumed mineral assemblage and proportion of rock and sediment in the calculation has the greatest effect on calculated Ca concentrations in pore waters. For example, at low temperatures there is a large discrepancy between 100% rock and 100% sediment contributions to dissolved Ca, likely due to the order of magnitude higher carbonate mineral concentrations in the sediment assemblage.

Yinazao Seamount, which is the closest to the trench of the three serpentinite seamounts sampled on IODP Exp. 366, has an estimated temperature in the upper basaltic basement of ∼80 °C (Hulme et al., 2010). At such temperatures the K modeled results cannot differentiate between basalt- or sediment-dominated reactions; however, the Ca and Na data show marked differences between calculated and measured data, suggesting the deep-sourced fluids at this site stem from a combination of basalt and sediment sources. Similarly, measured Na and Ca data from Fantangisna Seamount, which is further from the trench with a temperature in the subduction channel of ∼125 °C to 150 °C, are distinctly different from the basalt only calculation, suggesting a sedimentary component is required. In contrast, Asùt Tesoru Seamount, which is the furthest from the trench of the three serpentinite seamounts with a temperature of ∼250 °C in basement (Hulme et al., 2010), is consistent with calculations using a basalt assemblage. This suggests that the contribution from sediment sources decreases with increasing temperature and pressure in the subduction channel.

Our data shows that there is no requirement for slab fluids originating from a serpentinised portion of the subducting lithosphere (e.g. Manea et al., 2014). Instead our results indicate a change from fluid-rock interactions requiring some sediment input at shallowest depths (13–14 km) to an altered basalt assemblage controlling fluid-rock interactions at 18 + km depth, in line with the subduction of altered oceanic crust (McCaig et al., 2018). The subduction of seamounts adds to the primary heterogeneity of the subducting slab, and the main heterogeneity that may affect the mineralogical and chemical reactions ongoing at the subduction interface is the incorporation of carbonate dominated sediments associated with seamounts and OIB versus MORB basalts (Fryer et al., 2020). The results of our thermodynamic calculations indicate that subtle differences in chemistry of the subducting slab (OIB vs MORB), or indeed heterogeneity due to carbonate sediment subduction are not required to explain our porewater results. Instead the drivers for the changes we observe are the breakdown of sediments at the shallowest levels, followed by fluid-rock interactions dominated by basalt at ∼ 18 km, driven by fluid-rock interactions at increasing temperatures (Fig. 8). Na, Ca, and K concentrations of pore fluids are controlled dominantly by basalt-water interactions at ≥ 18 km depth. This finding may indicate that

sediment recycling in the Mariana subduction zone is largely limited to shallow depths beneath the forearc. However, more precise tracers of sediment–water interaction are required to investigate this further.

A rock-dominated scenario for the subduction interface (low water: rock ratio, see Supplementary Materials) is consistent with recent mineralogical assessments. For example, generation of anomalously high pH at the three deepest-sourced mud volcanoes, but lower than predicted H_2, and elevated CH_4 concentrations and very high alkalinities indicate that a reaction that conserves alkalinity and generates CH_4 may facilitate such extreme pH, and the reduction of bicarbonate is a likely candidate (Wheat et al, 2020) (*Eq. (1)*)

$$4H_2 \; + \; HCO_3^- \; \rightarrow CH_4 \; + \; 2H_2O \; + \; OH^- \tag{1}$$
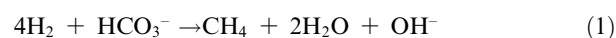
For such a reaction to proceed a source of carbon is required, likely from the breakdown of carbon-bearing minerals in the subducting slab, along with H_2 generated during serpentinisation in the mantle wedge. Abundant carbonate veining was recorded in metabasic and metasedimentary xenoliths/ clasts sampled from Fantangisna, Asùt Tesoru and Conical mud volcanoes, but none were observed from Yinazao, nor within serpentinite clasts (Albers et al, 2019). Microstructual analyses of these veins indicate that they are undeformed and detailed study of those from Asùt Tesoru shows they are in textural equilibrium with the blueschist facies mineral, lawsonite, indicating that they formed after deformation but during blueschist facies conditions at or near the subduction interface (Albers et al., 2019; Ichiyama et al., 2021). These observations are in agreement with the fluid geochemistry indicating that there is carbon mobility and deposition at > 18 km depth; >250 °C below Asùt Tesoru, South Chamorro and Conical serpentinite mud volcanoes.

Similarly the observed increase in dissolved Na concentrations in the deep-sourced fluid at these serpentinite mud volcanoes has been attributed to the transition from lawsonite-blueschist to epidote-blueschist facies (Maekawa et al. 1995; Mottl et al., 2008). Documentation of metabasic clast mineralogy identifies that this boundary would lie somewhere between 18 and 19 km depth, i.e. between Asùt Tesoru (containing lawsonite, Ichiyama et al., 2021) and South Chamorro (containing epidote, Tamblyn et al., 2019). The mineralogical and pore water data strongly suggests that the exact P-T conditions for this reaction, which are not well constrained experimentally, lie under these mud volcanoes at about 0.6 GPa and 250–300 °C.

The transformation of lawsonite to epidote at this transition follows (Wheat et al., 2020):

$$\text{Lawsonite} \; + \; Ca^{2+} \; + \; Na_2O \; (cpx) \; \rightarrow \; \text{Epidote} \; + \; 5H_2O \; + \; 2Na^+ \tag{2}$$
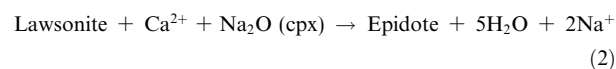
This reaction consumes Ca from, and liberates Na to the aqueous phase as well as producing H_2O that contributes to fluid freshening. Thermodynamic modelling indicates that this reaction is triggered at ∼ 220 °C for clinozoisite epidote endmember and causes an abrupt elevation in the Na/Ca ratio of associated fluids as epidote consumes Ca from solution, resulting in the generation of a carbonate-rich pore
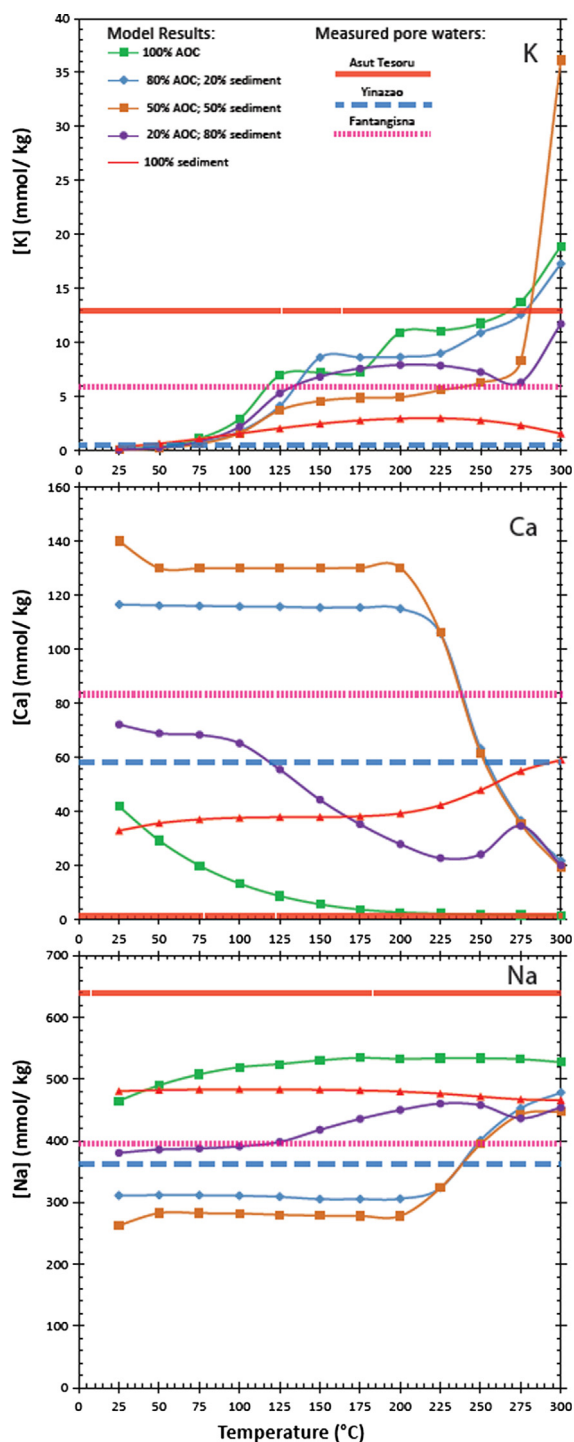
Fig. 8. PHREEQC modelled pore water major solute concentrations (K, Ca, Na) in equilibrium with different mineral assemblages (see Table S2) from 100% sediment to 100% basalt across the temperature range 25 °C to 300 °C. Deep-sourced concentrations based on measured pore water values from summit sites are shown as horizontal dashed lines, illustrating that such deep-sourced fluids could result from reactions with a range of sediment and altered oceanic crust (AOC) assemblages.

water (Mottl, 2009). Zoned garnets from Sifnos, Greece, which represent an exhumed subduction zone, display more oxidized cores and more reduced rims corresponding to lawsonite dehydration (Gerrits et al., 2019), and stable iron isotope signatures of serpentinite clasts from Mariana serpentinite mud volcanoes indicate oxidation of the mantle wedge is driven by oxidized slab carbonate or sulfate-bearing fluids (Debret et al., 2020). These studies provide independent evidence for the generation of oxidizing fluids under similar conditions to those under our deep-seated mud volcanoes, in particular during slab lawsonite breakdown. These studies indicate that the lawsonite-blueschist to epidote-blueschist transition is crucial in controlling where carbon is mobilized and where redox transfers from subducting slab to the mantle wedge occur.

Studies of exhumed portions of high and ultrahigh pressure metamorphic rocks interpreted to represent a residual subducting slab have shown that carbonates are stable to great depths (cf. 80–90 km) (Collins et al, 2015), and decarbonation of sedimentary and vein carbonate requires temperatures of > 400 to < 540 °C at 0.8 GPa (Kerrick and Connolly, 2001a, b). However, in the Mariana forearc we document evidence for widespread decarbonation of the subduction channel associated with the lawsonite-blueschist to epidote-blueschist transition at 250–300 °C and ~ 0.6 GPa, (of note this transition is poorly constrained experimentally at temperatures less than 300 °C owing to experimental limitations, Schmidt and Poli, 1994; 1998; Martin et al., 2014). Consequently, such carbonate breakdown must be driven by the consumption of Ca from solution by growing epidote on the prograde metamorphic pathway of the subducting slab. This pathway drives high fluid carbonate contents, facilitating Eq (2) and generating high pH (12.5), low Ca, high Na and CH_4, freshened pore waters. Although this work highlights where these reactions and carbon destabilization occurs in the Mariana forearc, we do not yet have a control on fluxes of such shallow carbon liberation and therefore the significance of these processes to global mass-balance models of the subducting slab remains enigmatic.

5.3. Dissolved gases

High concentrations of dissolved H_2, CH_4, C_2H_6, and C_3H_8 were observed in pore waters at the summit of Asùt Tesoru, and comparatively low but significant levels of these dissolved gases were detected at summit and flank sites on Fantangisna and Yinazao Seamounts. The variability in gas composition among the three examined seamounts indicates variation in deep serpentinization and fluid migration processes (Wheat et al., 2020). Dissolved H_2 versus CH_4 concentrations show two trends, reflecting a vigorous fluid discharge at the summit of Asùt Tesoru Seamount that is CH_4-enriched compared to the other two summit sites (Fig. 9). Data from the conduit of Asùt Tesoru Seamount show a linear correlation consistent with thermodynamic estimates of serpentinization-driven H_2 production

(McCollom and Bach, 2009), and concomitant CH_4 (hydrocarbon) production by abiotic (e.g., Fischer-Tropsch type) and/or thermogenic processes at or near the subduction interface (Eickenbusch et al., 2019). The relatively scattered trend of the other serpentinite seamounts may reflect variations in physical and chemical conditions, and/or microbial activity specifically related to CH_4 or H_2 consumption. When plotting the ratio of CH_4 vs $C_2H_6 + C_3H_8$ ($C_1/(C_2 + C_3)$ ratio), data from summit of Asùt Tesoru, Conical and South Chamorro Seamounts form a single linear trend (Fig. 9). This trend reflects a similar hydrocarbon production process in the subduction channel below. The $C_1/C_2 + C_3$ ratio (300–400) may be explained by either abiotic or thermogenic processes or by the combination of both. In addition, two different trends of C_1 versus $C_2 + C_3$ and $C_1/(C_2 + C_3)$ ratios are observed in data from the summit and flank sites of Fantangisña Seamount (Fig. 9), the latter have undergone post-depositional diagenetic reactions. The summit sites may be consistent with data from Asùt Tesoru, Conical and South Chamorro Seamounts, but the $C_1/(C_2 + C_3)$ ratios in flank data are significantly different, likely associated with abiotic and microbial processes specifically coupled with CH_4 that could be influenced by the pelagic sediment below the serpentinite cover.

5.4. Diagenesis of serpentinite and the underlying pelagic sediment

The three serpentinite seamounts that were drilled on IODP Exp. 366 are in different stages of activity, based on their morphology and systematic variations in pore water chemical data. Asùt Tesoro Seamount has a distinct summit knoll with two additional mounds with pore water seepage rates that are in excess of the mud matrix. These rates increase towards the middle of the summit mound (Hulme et al., 2010). Pore water profiles from the summit site (U1496) show, for example, linear relationships among conservative solutes such as Na, Li, K, Rb, and Cs (e.g., Fig. 5). For this site, fluid seepage is sufficiently fast such that the rate and flux of diagenetic reactions is small compared to the seepage flux, thus while such reactions may occur, there is insufficient time for such reactions to alter the deep-sourced fluid composition as it ascends. In this case even sulfate and alkalinity are conservative in the upwelling fluid at Site U1496.

Site U1495 is a flank site located about 2.2 km from the summit site (U1496) and roughly on the summit platform that supports the summit knoll. Here, pore water chemical compositions are generally conservative and point to a deep-sourced fluid composition. Given the chemical gradient with depth, the calculated concentration at about 25 mbsf matches the composition of the deep-sourced fluid (Fig. S1). Thus, the close proximity of the deep-sourced fluid to the seafloor and other data from the summit region (e.g., Hulme et al. (2010)) suggest that the 20 km^2 area of the summit region is active with the summit knoll the focus of current activity. Likewise, most of the other solutes at Site U1495 show a linear response with the K data, indicating two endmember mixing (deep-sourced fluid and bottom seawater) via advection and diffusion.

In contrast, pore water chemical relationships within the other two flank sites (U1493 and U1494) of Asùt Tesoro Seamount are more complicated. Some of the solutes at these sites are conservative. For example, in general, the alkali metals show a linear response with K data and show a linear relationship with depth (Figs. 5 and 6). If we expand this linear depth relationship to the intersection defined by the deep-sourced composition of K and Na, then the concentration-depth relationship would point to a depth of $\sim$ 110 to 120 m (Fig. S1). This concentration-depth relationship and the one in the previous paragraph provide a measure of the temporal affect of diffusion. If we simplify the diffusion equation by assuming a constant sediment diffusion coefficient, porosity, and formation factor that is related to the square of the porosity (e.g., Berner, 1980), then we can gauge when the cored serpentinite matrix formed, provided no seawater was incorporated into the serpentinite matrix during the mass wasting event (Supplementary Materials). This calculation results in a maximum time since deposition, which is around 20 ky for Site U1495 and $\sim$ 300 ky to 400 ky for Sites U1393 and U1394 (Fig. S1). If seawater was incorporated during mass wasting, then the effect would be to lessen the calculated length of time since the last event.

Other solute data from Sites U1493 and U1494 do not match the linear relationship defined by data from the summit site (U1496), indicating reaction within the serpentinite matrix, bottom seawater that is transported into the sediment via diffusion, potentially pelagic sediment. The latter may be present since serpentinite mud volcanoes are episodic maybe on time scales of hundreds of thousands of years or longer. Thus, pelagic sediment could deposit on the flanks and be mixed within or overlain during a mass-wasting event, consistent with the dissolved silica data that show higher values near the sediment–water interface. For example, sulfate concentrations decrease with depth, consistent with microbial sulfate reduction. Even though Sr and Ca are depleted in the deep-sourced fluid, their concentrations increase from $\sim$ 70% of the seawater concentration at the sediment–water interface to $\sim$ 120% of the seawater value at 20 mbsf. Over this range, measured fluid alkalinities drop from 0.9 mmol kg^{-1} (much lower than the value in bottom seawater, 2.4 mmol kg^{-1}) to 0.4 mmol kg^{-1}, even though the deep-sourced fluids have a composition of 73 mmol kg^{-1}. Combined, these data indicate a complex process that governs carbonate formation and dissolution. The boron data also indicate diagenetic reactions, showing a decrease in concentration from bottom seawater (410 μmol kg^{-1}) to 90 μmol kg^{-1} at $\sim$ 30 mbsf, while the deep-sourced fluid has a concentration of about 1,050 μmol kg^{-1} (Fig. 6).

Yinazao Seamount is less active than Asùt Tesoro Seamount as indicated by the lack of a summit knoll and slower pore water seepage rates (Hulme et al., 2010). The latter is significant in that even at the summit site many of the solutes are affected by reaction during ascent. This is not the case for Na, K, and Rb, which are generally conservative in this setting. As above, pore water K and Rb data from the flank site (U1491) would intersect the value of the deep-sourced fluid at a depth of 110 to 50 m, respectively, for Hole
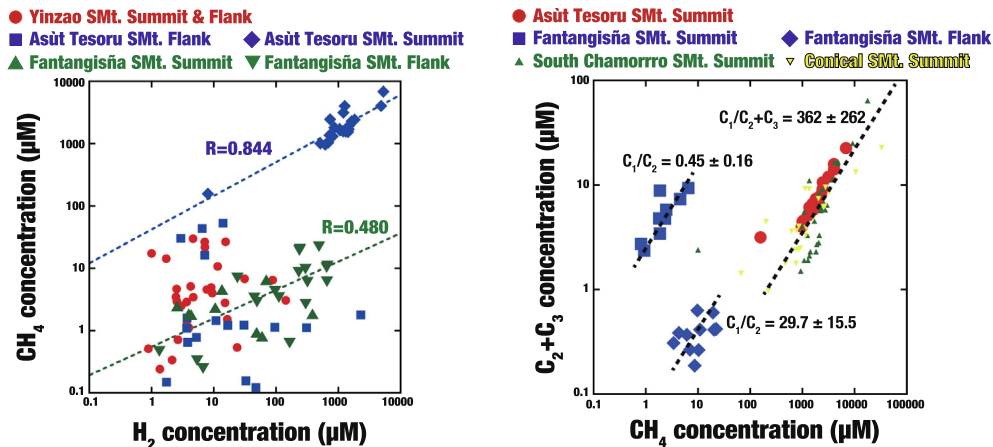
Fig. 9. A) H_2 vs CH_4 diagram in Yinazao and Asùt Tesoru Seamounts. Red circles indicate H_2 and CH_4 concentrations from the summit and flank sites of Asùt Tesoru Seamount and blue squares indicate those from the summit and flank sites of Yinazao Seamount. B) CH_4 vs C_2H_6 diagram for Asùt Tesoru, Conical and South Chamorro Seamounts. Red circles indicate CH_4 vs C_2H_6 concentrations from the summit and flank sites of Asùt Tesoru Seamount, blue squares and yellow diamonds indicate those from the summit and flank sites of Conical and South Chamorro. (For interpretation of the references to colour in this figure legend, the reader is referred to the web version of this article.)
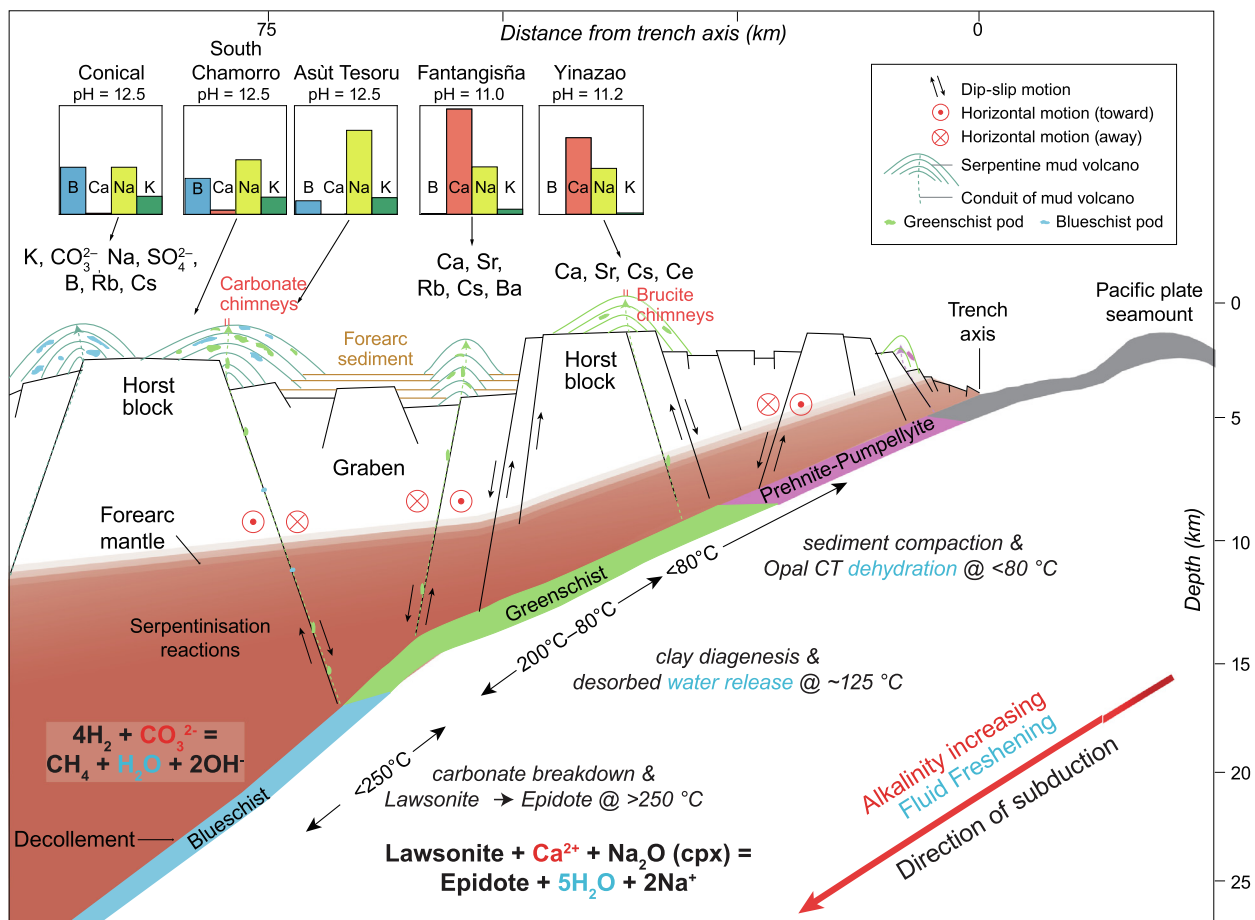

Fig. 10. Summary cross section of the Mariana convergent margin showing mud volcanoes referred to in this study drawn at appropriate distances from the trench, above estimated slab depth, but all translated to the same line of section for comparison. Note that the vertical and horizontal scales are not the same. The main changes in pore water chemistry with progressive subduction are outlined and related to mineral transformation and chemical reactions occurring at depth in the subduction channel. Figure modified from Fryer et al. (1999) and Fryer et al. (2018) including data from Hulme et al. (2010), Mottl et al. (2004), and this work.

U1491B and 240 to 80 m, respectively, for Hole U1491C. This corresponds to a range of 0.05 to 1.2 My of diffusive exchange with bottom seawater, should deposition not entrain bottom seawater. More importantly, though, is that for some solutes the relationship with K is not linear at the summit site (U1492), meaning that the solute is either consumed or produced during ascent. For example, during ascent at Site U1492, Sr and Ca are released from the serpentinite matrix to the deep-sourced fluid. In contrast, Mg, B, Si, U, Mo, and alkalinity are removed from the deep-sourced fluid during ascent. These exchanges occur in roughly the upper 5 m in Hole U1492C, the upper 10 m in Hole U1492B, and throughout the cored section (to 36 m) at Hole U1492A. The variation in depths is a function of the seepage rate, with a faster seepage rate at Hole U1492C. Exchange is observed because the seepage rate is sufficiently slow (Hulme et al., 2010) such that reactions, and the effect of diffusive exchange with seawater, impact the composition of the upwelling fluid.

These exchanges are not the same as those found on the flank site (U1491). Here, near-bottom seawater compositions are observed for several solutes and the dissolved silica data are consistent with reaction with pelagic sediment including sulfate reduction. Sr concentrations increase with depth, Ca concentrations remain constant, and the alkalinity decreases with depth consistent with carbonate exchange. Although B is nearly depleted in the deep-sourced fluid at this serpentinite mud volcano summit (U1492), B concentrations on the flanks increase with depth resulting from incongruent serpentine dissolution. These processes involved in serpentine diagenesis result in large boron and silicon isotope fractionation and changes in solute profiles with depth over time (Geilert et al., 2020).

Hole U1498A, closer to the toe of the flow, penetrated 53 m of serpentinite matrix and 128.6 m of underlying pelagic-volcanic sediment and Hole U1498B penetrated 205 m of serpentinite matrix and 55 m of pelagic-volcanic sediment. The deepest sample at 193 mbsl has a seawater Na concentration and a pH (25 °C) of 10.9 (down from 11.4 shallower in the section). A plot of Na versus K (Fig. S2) reveals a linear pattern for samples from Hole 1498B for all but the deepest three samples, which show higher Na concentrations for a given K concentration. The shape of the Na profile suggests that pore waters from the underlying pelagic-volcanic sediment have diffusively exchanged with pore waters in the serpentine matrix from the boundary at 205 mbsf to 134 mbsf, ~71 m above the serpentintite-sediment interface. Thus, the depositional event occurred at most 100,000 years ago, assuming the deposition did not entrain seawater. Similarly, pore waters from Hole U1498A, which recovered 53 m of serpentinite material, has seawater Na concentrations throughout the pore water profile and a maximum pH (25 °C) of 8.7 centered at 37.6 mbsf. Such profiles would be affected by diffusion from the underlying sediment and the overlying seawater. The difference in composition between the two holes is also observed in Rb, Li, and Cs data where linear relationships with K from Site U1497 at the summit are matched with data from Hole U1498B, but not from Hole U1498A. As anticipated, diffusive exchange with bottom seawater and underlying pelagic sediment has a greater impact on the thinner section of serpentinite material to the point of drastically diminishing the pH (25 °C) by almost three orders of magnitude.

6. CONCLUSIONS

IODP Expedition 366 cored three serpentinite mud volcanoes in the Mariana Forearc with coring operations that were undertaken at summit sites and on the flanks. At one flank site (Fantagnisna Seamount) the underlying pelagic sediment below the serpentinite matrix was recovered. Pore waters were extracted from the serpentinite matrix revealing the composition of the deep-sourced fluid that is consistent with earlier assessments over a larger number of sampled serpentinite seamounts (e.g. Hulme et al, 2010; Mottl et al., 2004) (Fig. 10). Distance from the trench has typically been used as a proxy for depth to and temperature of the subduction channel; however, the non-homogeneous nature of the subducting Pacific Plate upsets this proxy. Instead we use the concentration of K in the deep-sourced fluid as a measure of temperature, because the only source of K to seep-sourced fluids is the downgoing slab, and water–rock reactions have a distinct effect on K concentrations. Thus, K acts as a suitable proxy for depth-to-slab even in locations were seamounts have disrupted the subduction process. Plotting the deep-sourced fluid K concentrations versus those of other solutes (e.g., B, Rb, Sr, Ca, Na, Na/Cl,) reveals monotonic trends, that indicate a temperature dependence on their release from the subducting slab.

Results from thermodynamic modelling for the shallowest-depths-to-slab reactions from ∼ 80–125 °C to over 250 °C are consistent with observed trends in deep-sourced fluids. The respective roles of fluid-rock reactions with sediments and/or basalt of the Pacific Plate in the subduction channel is constrained using this initial approach. Comparing the modeled and observed results suggest that a sediment-derived component to the deep-source fluid is likely at cooler temperatures (<150 °C), but at higher temperatures (>250 °C) the deep-sourced fluid is likely dominated by basalt-water reactions. The involvement of other potential slab constituents (e.g., lithospheric serpentinite, carbonate-rich sediments, OIB-like seamount basalts) are not required to explain our results.

At >250 °C metamorphic transformations control the solute load of liberated fluids. Our modeling coupled with recent mineralogical studies highlight the importance of the transformation of lawsonite to epidote. This transformation releases Na to deep-sourced fluids while removing Ca, which in turn drives carbonate dissolution producing bicarbonate, which reacts with hydrogen liberated from serpentinization to produce the observed high pH, methane-bearing fluids. Dissolved methane concentrations in the deep-sourced fluids do not show the monotonic trends across the forearc seen in K and other mobile species. However, at temperatures in the subduction channel in excess of 250 °C, the CH_4 vs $C_2H_6 + C_3H_8$ ($C_1/(C_2 + C_3)$ ratio) is consistent among Asùt Tesoru, Conical and South Chamorro Seamounts, highlighting a temperature barrier and thermodynamic controls over hydrocarbon productivity.

Pore waters that were recovered from materials on the flanks of the mud volcanoes show conservative behavior for some solutes (e.g., Na, Li, K, Rb, and Cs) and evidence for ongoing reactions from other solutes. Conservative solutes can be used to constrain the depositional history of flank deposits, assuming a simplistic view of serpentinite mass wasting and deposition without the entrainment of bottom seawater. Nevertheless deposition events on the flanks may be on the scale of tens of thousands of years to a million years during which time diagenetic reactions continue, drastically lowering the pH and affecting major and trace element compositions alike. This initial assessment highlights the necessity for diagenetic reactions within the serpentinite matrix after deposition on the flanks and the potential for biogeochemical reactions in this high pH environment.

This work and other data generated during the expedition provide a foundation for more directed studies that address the four goals of the drilling program. Isotopic evidence has proved insightful to, for example, elucidate the Si cycle (Geilert et al., 2020). A component of the expedition was the installation of borehole observatories, which will be used to better address systematics of dissolved gases and low molecular weight organics especially for those sites that are cooler and closer to the trench where decarbonization driven by lawsonite to epidote breakdown is not dominant. Such studies will help define transport and alteration within the early stages of subduction.

Declaration of Competing Interest

The authors declare that they have no known competing financial interests or personal relationships that could have appeared to influence the work reported in this paper.

SUPPLEMENTARY MATERIAL

Supplementary data to this article can be found online at https://doi.org/10.1016/j.gca.2021.10.030.

REFERENCES

Albers E., Bach W., Klein F., Menzies C. D., Lucassen F. and Teagle D. A. H. (2019) Fluid-rock interactions in the shallow Mariana forearc: carbon cycling and redox conditions. *Solid Earth* **10**, 907–930.

Albers E., Kahl W.-A., Beyer L. and Bach W. (2020) Variant across-forearc compositions of slab-fluids recorded by serpentinites: Implications on the mobilization of FMEs from an active subduction zone (Mariana forearc). *Lithos* **364–365** 105525.

Alt J. C. and Teagle D. A. H. (1999) The uptake of carbon during alteration of ocean crust. *Geochim. Cosmochim. Acta* **63**(10), 1527–1535.

Barnes I. and O'Neil J. R. (1969) The Relationship between Fluids in Some Fresh Alpine-Type Ultramafics and Possible Modern Serpentinization, Western United States. *Geol. Soc. Am. Bull.*, 1947–1960.

Bebout G. E. (2007) Metamorphic chemical geodynamics of subduction zones. *Earth Planet. Sci. Lett.* **260**(3), 373–393.

Bebout G. E., Bebout A. E. and Graham C. M. (2007) Cycling of B, Li, and LILE (K, Cs, Rb, Ba, Sr) into subduction zones: SIMS evidence from micas in high-P/T metasedimentary rocks. *Chem. Geol.* **239**(3–4), 284–304.

Berner R. A. (1980) Early Diagenesis. Princeton Univ. Press (21st August, 1980), 241 pp.

Collins N. C., Bebout G. E., Angiboust S., Agard P., Scambelluri M., Crispini L. and John T. (2015) Subduction zone metamorphic pathway for deep carbon cycling: II. Evidence from HP/UHP metabasaltic rocks and ophicarbonates. *Chem. Geol.* **412**, 132–150.

Debret B., Reekie C. D. J., Mattielli N., Beunon H., Ménez B., Savov I. P. and Williams H. M. (2020) Redox transfer at subduction zones: insights from Fe isotopes in the Mariana forearc. *Geochem. Perspect. Lett.* **12**, 46–51.

Eickenbusch E., Takai K., Sissmann O., Suzuki S., Menzies C. D., Sakai S., Sansjofre P., Tasumi E., Bernasconi S. M., Glombitza C., Jørgensen B. B., Morono Y. and Lever M. A. (2019) Origin of Short-Chain Organic Acids in Serpentinite Mud Volcanoes of the Mariana Convergent Margin. *Front. Microbiol.* **10**, 1729.

Fryer P. (1996) Evolution of the Mariana Convergent Plate Margin System. *Rev. Geophys.* **34**(1), 89–125.

Fryer P. (2012) Serpentinite Mud Volcanism: Observations, Processes, and Implications. *Ann. Rev. Marine Sci.* **4**(1), 345–373.

Fryer P. and Fryer G. J. (1987) Origins of Nonvolcanic Seamounts in a Forearc Environment, Seamounts, Islands. In *and Atolls*. American Geophysical Union, pp. 61–69.

Fryer P., Wheat C. G. and Mottl M. J. (1999) Mariana blueschist mud volcanism: Implications for conditions within the subduction zone. *Geology* **27**(2), 103–106.

Fryer, P., Wheat, C. G., Williams, T., Albers, E., Bekins, B., Debret, B. P. R., Jianghong, D., Yanhui, D., Eickenbusch, P., Frery, E. A., Ichiyama, Y., Johnson, K., Johnston, R. M., Kevorkian, R. T., Kurz, W., Magalhaes, V., Mantovanelli, S. S., Menapace, W., Menzies, C. D., Michibayashi, K., Moyer, C. L., Mullane, K. K., Park, J.-W., Price, R. E., Ryan, J. G., Shervais, J. W., Suzuki, S., Sissmann, O. J., Takai, K., Walter, B., and Rui, Z., 2018, Proceedings of the International Ocean Discovery Program; Mariana convergent margin and South Chamorro Seamount; Expedition 366 of the riserless drilling platform, Guam to Hong Kong; Sites 1200 and U1491-U1498, 8 December 2017-7 February 2017, Washington, DC, United States, International Ocean Discovery Program. 10.14379/iodp.proc.366.2018.

Fryer P., Wheat C. G., Williams T., Kelley C., Johnson K., Ryan J., Kurz W., Shervais J., Albers E., Bekins B., Debret B., Deng J., Dong Y., Eickenbusch P., Frery E., Ichiyama Y., Johnston R., Kevorkian R., Magalhaes V., Mantovanelli S., Menapace W., Menzies C., Michibayashi K., Moyer C., Mullane K., Park J.-W., Price R., Sissmann O., Suzuki S., Takai K., Walter B., Zhang R., Amon D., Glickson D. and Pomponi S. (2020) Mariana serpentinite mud volcanism exhumes subducted

seamount materials: implications for the origin of life: Philosophical Transactions of the Royal Society A: Mathematical. *Phys. Eng. Sci.* **378**(2165), 20180425.

Fryer P., Pearce J. A., Stokking L. B., et al. (1990) Proc. ODP, Init. Repts., 125: College Station, TX (Ocean Drilling Program). doi: 10.2973/odp.proc.ir.125.1990.

Fryer, P.B., Salisbury, M.H., 2006, Leg 195 synthesis; Site 1200; serpentinite seamounts of the Izu-Bonin/Mariana convergent plate margin, ODP Leg 125 and 195 drilling results: Proceedings of the Ocean Drilling Program; scientific results; seafloor observatories and the Kuroshio Current; covering Leg 195 of the cruises of the drilling vessel JOIDES Resolution; Apra Harbor, Guam, to Keelung, Taiwan; Sites 1200-1202; 2 March-2 May 2001, 195, 30.

Geilert S., Grasse P., Wallmann K., Liebetrau V. and Menzies C. D. (2020) Serpentine alteration as source of high dissolved silicon and elevated δ30Si values to the marine Si cycle. *Nat. Commun.* **11**, 5123.

Gerrits A. R., Inglis E. C. and Dragovic B., et al. (2019) Release of oxidizing fluids in subduction zones recorded by iron isotope zonation in garnet. *Nat. Geosci.* **12**, 1029–1033.

Gieskes, J.M., Gamo, T., Brumsack, H., 1991. Chemical methods for interstitial water analysis aboard JOIDES Resolution: Ocean Drilling Program Texas A&M University Technical Note, 15, 1–60.

Henstock T. J., McNeill L. C. and Tappin D. R. (2006) Seafloor morphology of the Sumatran subduction zone: Surface rupture during megathrust earthquakes? *Geology* **34**(6), 485–488.

Hulme S. M., Wheat C. G., Fryer P. and Mottl M. J. (2010) Pore water chemistry of the Mariana serpentinite mud volcanoes: A window to the seismogenic zone. *Geochem. Geophys. Geosyst.* **11**(1), p. n/a-n/a.

Ichiyama Y., Tsujimori T., Fryer P., Michibayashi K., Tamura A. and Morishita T. (2021) Temporal and spatial mineralogical changes in clasts from Mariana serpentinite mud volcanoes: Cooling of the hot forearc-mantle at subduction initiation. *Lithos* **384–385** 105941.

James R. H., Allen D. E. and Seyfried, Jr, W. E. (2003) An experimental study of alteration of oceanic crust and terrigenous sediments at moderate temperatures (51 to 350°C): insights as to chemical processes in near-shore ridge-flank hydrothermal systems. *Geochim. Cosmochim. Acta* **67**(4), 681–691.

Kerrick D. M. and Connolly J. A. D. (2001a) Metamorphic devolatilization of subducted marine sediments and the transport of volatiles into the Earth's mantle. *Nature* **411**(6835), 293–296.

Kerrick D. M. and Connolly J. A. D. (2001b) Metamorphic devolatilization of subducted oceanic metabasalts: implications for seismicity, arc magmatism and volatile recycling. *Earth Planet. Sci. Lett.* **189**(1), 19–29.

Kessel R., Schmidt M. W., Ulmer P. and Pettke T. (2005) Trace element signature of subduction-zone fluids, melts and supercritical liquids at 120–180 km depth. *Nature* **437**(7059), 724–727.

Klein F. and Le Roux V. (2020) Quantifying the volume increase and chemical exchange during serpentinization. *Geology* **48**, 552–556.

Maekawa H., Shozul M., Ishll T., Fryer P. and Pearce J. A. (1993) Blueschist metamorphism in an active subduction zone. *Nature* **364**, 520–523.

Maekawa H., Fryer P. and Ozaki A. (1995) Incipient Blueschist-Facies Metamorphism in the Active Subduction Zone Beneath the Mariana Forearc, Active Margins and Marginal Basins of the Western Pacific. *Am. Geophys. Union*, 281–289.

Manea V. C., Leeman W. P., Gerya T., Manea M. and Zhu G. (2014) Subduction of fracture zones controls mantle melting and geochemical signature above slabs. *Nat. Commun.* **5**, 5095.

Marschall H. R., Pogge von Strandmann P. A. E., Seitz H.-M., Elliott T. and Niu Y. (2007) The lithium isotopic composition of orogenic eclogites and deep subducted slabs. *Earth Planet. Sci. Lett.* **262**(3–4), 563–580.

Martin L. A. J., Hermann J., Gauthiez-Putallaz L., Whitney D. L., Vitale Brovarone A., Fornash K. F. and Evans N. J. (2014) Lawsonite geochemistry and stability – implication for trace element and water cycles in subduction zones. *J. Metamorph. Geol.* **32**, 455–478.

McCaig A. M., Titarenko S. S., Savov I. P., Cliff R. A., Banks D., Boyce A. and Agostini S. (2018) No significant boron in the hydrated mantle of most subducting slabs. *Nat. Commun.* **9**, 4602.

McCollom T. M. and Bach W. (2009) Thermodynamic constraints on hydrogen generation during serpentinization of ultramafic rocks. *Geochim. Cosmochim. Acta* **73**(3), 856–875.

Moore J. C. and Saffer D. (2001) Updip limit of the seismogenic zone beneath the accretionary prism of Southwest Japan: An effect of diagenetic to low-grade metamorphic processes and increasing effective stress. *Geology* **29**(2), 183–186.

Mottl M. J. (2009) Highest pH? *Geochemical News* **141**.

Mottl, M.J., 1992, Pore waters from serpentinite seamounts in the Mariana and Izu-Bonin forearcs, Leg 125: evidence for volatiles from the subducting slab, 1992, In Fryer, P., Pearce, J.A., Stokking, L.B., et al., Proceedings of the Ocean Drilling Program, Scientific Results, 125, 373–385.

Mottl M. J., Komor S. C., Fryer P. and Moyer C. L. (2003) Deep-slab fluids fuel extremophilic Archaea on a Mariana forearc serpentinite mud volcano: Ocean Drilling Program Leg 195. *Geochem. Geophys. Geosyst.* **4**, no. 11.

Mottl M. J., Wheat C. G., Fryer P., Gharib J. and Martin J. B. (2004) Chemistry of springs across the Mariana forearc shows progressive devolatilization of the subducting plate. *Geochim. Cosmochim. Acta* **68**(23), 4915–4933.

Mottl, M. J., McCollom, T. M., Wheat, C. G., Fryer, P. 2008 Decarbonation of the Subducting Pacific Plate Triggered by the Lawsonite-to-Epidote Transition Beneath the Mariana Forearc Serpentinite Mud Volcanoes American Geophysical Union Fall Meeting 15-19th December 2008, U51C-0

Murata K., Maekawa H., Yokose H., Yamamoto K., Fujioka K., Ishii T., Chiba H. and Wada Y. (2009) Significance of serpentinization of wedge mantle peridotites beneath Mariana forearc, western Pacific. *Geosphere* **5**, 90–104.

Murray R. W., Miller D. J. and Kryc K. A. (2000) Analysis of major and trace elements in rocks, sediments, and interstitial waters by inductively coupled plasma–atomic emission spectrometry (ICP-AES): ODP Tech. *Note* **19**.

Oakley A. J., Taylor B., Fryer P., Moore G. F., Goodliffe A. M. and Morgan J. K. (2007) Emplacement, growth, and gravitational deformation of serpentinite seamounts on the Mariana forearc. *Geophys. J. Int.* **170**(2), 615–634.

Oakley A. J., Taylor B. and Moore G. F. (2008) Pacific Plate subduction beneath the central Mariana and Izu-Bonin fore arcs: New insights from an old margin. *Geochem. Geophys. Geosyst.* **9**, no. 6.

Parkhurst D. L. and Appelo C. A. J. (1999) *User's Guide to PHREEQC (Version 2): A Computer Program for Speciation, Batch-Reaction, One-Dimensional Transport, and Inverse Geochemical Calculations.* United States Geological Survey, Water-Resources Investigations Report, pp. 99–4259.

Plank T., Ludden J. N., Escutia C., et al. (2000) Proc. ODP, Init. Repts., 185: College Station, TX (Ocean Drilling Program). doi:10.2973/odp.proc.ir.185.2000.

Plank T. and Manning C. E. (2019) Subducting carbon. *Nature* **574** (7778), 343–352.

Ryan J. G. and Chauvel C. (2014) 3.13 - The Subduction-Zone Filter and the Impact of Recycled Materials on the Evolution of the Mantle. In *Treatise on Geochemistry (Second Edition): Oxford* (eds. H. D. Holland and K. K. Turekian). Elsevier, pp. 479–508.

Salisbury, M.H., Shinohara, M., Richter, C., et al., 2002. *Proc. ODP, Init. Repts.,* 195: College Station, TX (Ocean Drilling Program). doi: 10.2973/odp.proc.ir.195.2002.

Savov I. P., Ryan J. G., D'Antonio M., Kelley K. and Mattie P. (2005) Geochemistry of serpentinized peridotites from the Mariana Forearc Conical Seamount, ODP Leg 125: Implications for the elemental recycling at subduction zones. *Geochem. Geophys. Geosyst.* **v. 6, no. 4**.

Schmidt M. W. and Poli S. (2014) 4.19 - Devolatilization During Subduction. In *Treatise on Geochemistry (Second Edition): Oxford* (eds. H. D. Holland and K. K. Turekian). Elsevier, pp. 669–701.

Schmidt M. W. and Poli S. (1998) Experimentally based water budgets for dehydrating slabs and consequences for arc magma generation. *Earth Planet. Sci. Lett.* **163**, 361–379.

Schmidt M. W. and Poli S. (1994) The stability of lawsonite and zoisite at high pressures: Experiments in CASH to 92 kbar and implications for the presence of hydrous phases in subducted lithosphere. *Earth Planet. Sci. Lett.* **124**, 105–118.

Seyfried W. E. and Bischoff J. L. (1979) Low temperature basalt alteration by sea water: an experimental study at 70°C and 150° C. *Geochim. Cosmochim. Acta* **43**(12), 1937–1947.

Seyfried W. E., Foustoukos D. I. and Fu Q. (2007) Redox evolution and mass transfer during serpentinization: An experimental and theoretical study at 200°C, 500bar with implications for ultramafic-hosted hydrothermal systems at Mid-Ocean Ridges. *Geochim. Cosmochim. Acta* **71**(15), 3872–3886.

Stern R. J. and Smoot N. C. (1998) A bathymetric overview of the Mariana forearc. *Isl. Arc* **7**(3), 525–540.

Tamblyn R., Zack T., Schmitt A. K., Hand M., Kelsey D., Morrissey L., Pabst S. and Savov I. P. (2019) Blueschist from the Mariana forearc records long-lived residence of material in the subduction channel. *Earth Planet. Sci. Lett.* **519**, 171–181.

Tatsumi Y. and Eggins S. (1995) *Subduction Zone Magmatism*. MA, Blackwell Science, Boston.

Wheat C. G., Fryer P., Fisher A. T., Hulme S., Jannasch H., Mottl M. J. and Becker K. (2008) Borehole observations of fluid flow from South Chamorro Seamount, an active serpentinite mud volcano in the Mariana forearc. *Earth Planet. Sci. Lett.* **267**(3–4), 401–409.

Wheat C. G., Seewald J. S. and Takai K. (2020) Fluid transport and reaction processes within a serpentinite mud volcano: South Chamorro Seamount. *Geochim. Cosmochim. Acta* **269**, 413–428.

Wheat, C.G., Fournier, T., Paul, C., Menzies, C.D., Price, R.E., Ryan, J., Sissmann, O. 2018, Data report: IODP Expedition 366 pore water trace element (V, Mo, Rb, Cs, U, Ba, and Li) compositions, Fryer, P., Wheat, C.G., Williams, T., and the Expedition 366 Scientists, Mariana Convergent Margin and South Chamorro Seamount., Volume 366: College Station, TX (International Ocean Discovery Program), Proceedings of the International Ocean Discovery Program.

You C. F., Castillo P. R., Gieskes J. M., Chan L. H. and Spivack A. J. (1996) Trace element behavior in hydrothermal experiments: Implications for fluid processes at shallow depths in subduction zones. *Earth Planet. Sci. Lett.* **140**(1–4), 41–52.

Associate Editor: Frieder Klein